PROCEEDINGS OF SCIENCE

Enhanced star formation in Narrow Line Syfert 1 galaxies

Elonora Sani*
Osservetorio Astrofisico di Arcetri, L. Fermi 5, 50125 Firenze-Italy
E-mail: sani@arcetri.astro.it

Dieter Lutz
2Max-Planck-Institut für extraterrestrische Physik, Postfach 1312, 85741 Garching, Germany
E-mail: lutz@mpe.mpg.de

Guido Risaliti
Osservetorio Astrofisico di Arcetri, L. Fermi 5, 50125 Firenze-Italy
E-mail: risaliti@arcetri.astro.it

Hagai Netzer
School of Physics and Astronomy and the Wise Observatory, The Raymond and Beverly Sackler Faculty of Exact Sciences, Tel-Aviv University, Tel-Aviv 69978, Israel
*E-mail:*netzer@wise.tau.ac.il

Lugi Gallo
Department of Astronomy & Physics, Saint Mary 's University, 923 Robie Street, Halifax, NS B3H 3C3, Canada
*E-mail:*lgallo@ap.smu.ca

Benny Trakhtenbrot
School of Physics and Astronomy and the Wise Observatory, The Raymond and Beverly Sackler Faculty of Exact Sciences, Tel-Aviv University, Tel-Aviv 69978, Israel
*E-mail:*trakht@wise.tau.ac.il

Eckhard Sturm
2Max-Planck-Institut für extraterrestrische Physik, Postfach 1312, 85741 Garching, Germany
E-mail: sturm@mpe.mpg.de

Thomas Boller
2Max-Planck-Institut für extraterrestrische Physik, Postfach 1312, 85741 Garching, Germany
E-mail: bol@mpe.mpg.de

PoS(NLS1)010

PROCEEDINGS OF SCIENCE

We present new Spitzer mid-IR spectroscopy of local NLS1s. We detect strong AGN continuum in all and clear PAH emission in 70% of the sources. The PAH luminosity spans three orders of magnitude, from $\sim 10^{39}$ to $\sim 10^{42}$ erg/s, providing strong evidence for intense ongoing star formation in the circumnuclear regions of NLS1s. We constructed NLS1 and BLS1 subsamples to compare them in various ways. The comparison shows a clear separation according to FWHM such that objects with narrower broad Hβ lines are the strongest PAH emitters. We test this division in various ways trying to remove biases due to luminosity and aperture size. We find that star formation activity around NLS1 AGN is larger than around BLS1 of the same AGN luminosity. The above result seems to hold over the entire range of distance and luminosity. Moreover, the star formation rate is higher in low black hole mass and high L/LEdd systems indicating that black hole growth and star formation are occurring simultaneously.

Narrow-Line Seyfert 1 Galaxies and their place in the Universe - NLS1,
April 04-06, 2011
Milan Italy

*Speaker.

PoS(NLS1)010

1. Introduction

Narrow Line Seyfert 1 galaxies (NLS1) have been considered in several works in the phase of building up their central black hole (BH). For example, NLS1s have lower BH masses compared with broad line Seyfert 1 galaxies (BLS1) of similar luminosity [1]. Translating their accretion rate and BH mass to L/L_{Edd} one finds that they are at the high end of the AGN distribution showing $L/L_{Edd} \simeq 1$ [2]. Moreover, they are the local counterpart of high redshift galaxies lying in the high accretion rate and high metallicity of the metallicity vs accretion rate diagram [3]. The large accretion rate and high metallicity of NLS1s are likely related to the presence of active star-forming regions in the hosts of such sources and Mathur [4] suggested that NLS1 live in rejuvenated, gas-rich galaxies with ongoing star formation (SF). This has been speculated in several individual sources with an ULIRG IR nature, but has not been shown to be the case in large NLS1s samples.

In the present work, we want to obtain a detailed mid-infrared (MIR) spectroscopic characterization of circumnuclear regions in the hosts of NLS1s. The aims are to investigate the possibility that such hosts show more intense SF compared with other AGN and to check the various relationships between SF and BH accretion. The high sensitivity and resolution of the Infrared Spectrograph (IRS) on board the Spitzer Space Telescope provide a most suitable tool to achieve these goals by obtaining high signal-to-noise ratio (S/N) low-resolution 5-15 μm spectra of many NLS1s. In particular, we want to characterize the SF in such systems using observations of polycyclic aromatic hydrocarbons (PAH) features that are superimposed on the strong MIR AGN continuum. The analysis of the SF-BH activity connection can then be carried out using a comparison sample of BLS1 of comparable luminosity.

2. Sample selection

We first extracted all the NLS1s and BLS1s from the 12^{th} edition of the Catalog of Quasars and Active Nuclei compiled by Véron-Cetty & Véron (hereafter VQC06) [5], using both catalogs of faint (i.e. Seyfert galaxies fainter than absolute magnitude $M = 23$) and bright AGNs (i.e. quasars brighter than $M = 23$). We probed for 'S1n' and for 'S1' or 'S1.0' or 'S1.2' classifications in VQC06, respectively. The defining criterion for inclusion as an NLS1 in the VQC06 is FWHM(Hβ)$\leq$ 2000 km/s. To assure high quality spectra, and to reduce aperture effects (see below) we used an upper redshift limit of $z \leq 0.2$. The final samples cover six orders of magnitude in luminosity. Among the BLS1s listed in VQC06, we excluded sources with Seyfert subclasses 1.5, 1.8 and 1.9. This is done to avoid confusion between NLS1s and BLS1s with particularly strong narrow lines, and possible intrinsic differences between Type 1 and Type 2 objects. We verified VQC06 spectral classifications from the literature or from SDSS DR7 spectra, eliminating a number of objects classified as S1 (1.0 or 1.2) in VQC06 but in fact corresponding to intermediate types lacking detectable BLR emission in Hβ.

Radio loudness is another potential bias. Synchrotron emission in radio loud (RL) AGNs can extend to shorter wavelengths and significantly contribute to the observed MIR continuum. This will dilute the hot-dust produced continuum and affect the relative strength of the observed PAH features. We therefore exclude RL sources from our sample.

The two lists thus defined were cross-checked against the Science Data Archive of the Spitzer Science Center (SSC) using the *Leopard* Archive Tool version 18.2 for selecting objects observed in the IRS Low Resolution Mode.

3. Data analysis

We decomposed the AGN and SF contribution to the observed spectrum by fitting the 5.5-6.85μm rest wavelength range of the spectra with a simple model of a linear continuum representing thermal emission by AGN-heated dust and a starburst template obtained from the ISO/SWS spectrum of M82. The latter is designed to enable a reliable measure of the 6.2μm PAH emission feature in the spectrum. We note that the broad wavelength MIR spectrum of luminous AGNs [6] is well represented by a linear or power-law continuum over the limited wavelength range considered here.

The fit parameters obtained in this way were used to calculate the rest frame 6 μm pure AGN flux density and the 6.2 μm PAH flux. The latter is obtained by integrating over the rest wavelength range 6.1-6.35 μm. The detection criterion for both the AGN continuum and the 6.2 μm PAH feature was fixed at a 3 σ level, and the error estimates are based on propagating the noise estimated from the difference of spectrum and fit over the rest wavelength range 5.5-6.85 μm. Cases of non-detections were assigned a 3 σ continuum and/or PAH upper limit. All fluxes were converted to luminosities which are referred to later on as L(6μm) and L(6.2 PAH).

4. Results

The results of our analysis are shown in Figure 1, and are summarized below:
- The PAH feature for star formation are detected in 70 % of NLS1s and 45 % of BLS1s.
- The comparison between unbiased NLS1 and BLS1 samples shows how the two population are separated and that NLS1 host more intense Starburst activity than BLS1. Possible luminosity and distance effects are carefully taken into account in the following discussion.

To quantify the contribution of SF regions to the NLS1 and BLS1 spectra we define the SF-AGN ratio R by

$$R = \frac{L(6.2, PAH)}{\nu L_\nu(6, AGN)}. \tag{4.1}$$

R is proportional to the PAH equivalent width (EW) measured against the pure AGN continuum. The correlation of R vs. FWHM(Hβ) is plotted in the left panel of Fig. 1, while histograms in the right panel show the distribution of R for NLS1 and BLS1.

Visual inspection of Fig. 1 suggests that NLS1s are characterized by larger R which can be interpreted as larger relative SF contribution to their MIR spectra. In particular the histogram points out a greater PAH detection rate in NLS1 than BLS1, and, most of all, that the majority of these detections correspond to the strongest circumnuclear SF activity (R$>$1). On the other hand R values for BLS1 are mostly upper limits, and the detections typically lie in the intermediate R rage (0.1$<$R$<$1).
This impression is substantiated by a formal censored statistical analysis performed on the data. We used an improved version of the logrank test, which correctly treats left-censored data. For

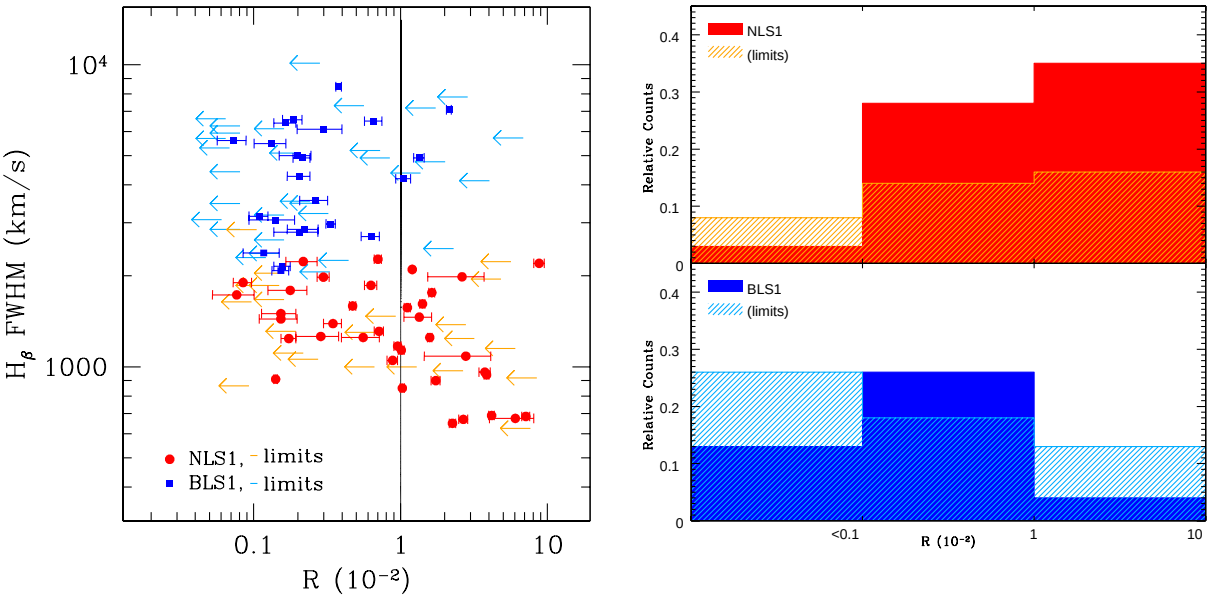

Figure 1: FWHM(Hβ) vs the PAH to continuum ratio R (defined in §4). Arrows indicate upper limits. Red dots are NLS1 whose upper limits are in orange. Blue squares are BLS1 with sky-blue limits. *Left panel*: the bidimensional plot displays the measurements and the black vertical line divides sources with strong SF (R>1) from the rest of the sample. *Right panel*: the R relative counts (limits) distribution is shown for both the NLS1 and BLS1 samples. The distribution is shown in bins for the three R orders of magnitude, relative to the proper sample number of sources.

the purpose of the analysis we divided the sample in two assuming in Fig. 1 a dividing line of FWHM(Hβ)= 2000 km/s, and compare their properties with respect to R. This gave a negligible probability (6×10^{-5}) that the two sub-samples are drawn from the same parent distribution. Moving the dividing line up or down by 100 km/s did not change the conclusion. This significant difference between NLS1 and BLS1 groups indicates that type-I AGNs with narrower broad emission lines reside in hosts containing more luminous SF regions.

While the above is the main finding of the present paper, there are several potential effects that could bias this result and lower its significance. The two most important ones are aperture and luminosity effects. The first depends on the source distance and is the result of the fixed size Spitzer slit width that includes more host galaxy light in more distance sources. The IRS slit width is 3.6" for the spectral range used here, i.e 3.5 kpc at a typical distance of 200 Mpc. This can result in larger R (more PAH emission) at higher redshifts. The second potential bias is related to the well-know increase in L(PAH) with AGN luminosity. The dependence of the two has been investigated in several samples (e.g. [6]) and, while linear, the slope is not 1 which can introduce a trend of R with AGN luminosity. Our NLS1 and BLS1 samples where not chosen on the basis of their similar distances or AGN luminosity, and thus the above issues may affect the trend seen in Fig. 1.

To investigate the potential influence of source distance and luminosity on the R vs. FWHM(Hβ) correlation in a way that fully includes the PAH nondetections, we have derived composite spectra of NLS1s and BLS1s in different luminosity-distance regimes. This was achieved by dividing the

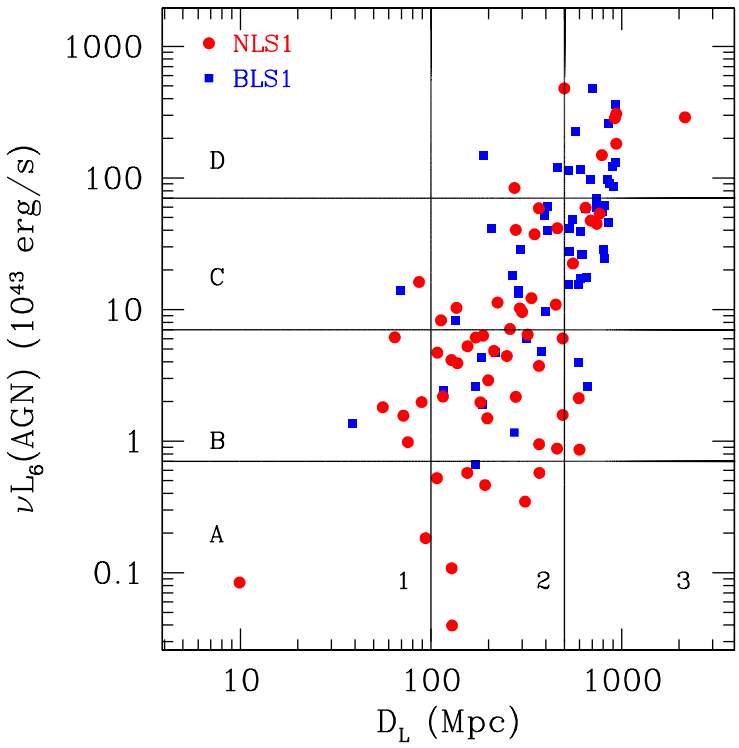

Figure 2: Luminosity-Distance diagram. The 10 regions shown are defined considering the AGN luminosity and redshift orders of magnitude.

entire luminosity-distance space into ten regions defined by sampling the luminosity range in four equally spaced bins of the size of one order of magnitude, and the distance axis in three zones spacing the redshift range in bins of one order of magnitude each. This corresponds to distance thresholds of 100 and 500 Mpc and AGN luminosity limits of 7×10^{42}, 7×10^{43} and 7×10^{44} erg/s. The ten zones and the distribution of NLS1s and BLS1s in them are shown in Fig. 2. We then obtained stacked spectra of all the NLS1s in each zone and compared them with stacked spectra of all the BLS1s in the same zone. The spectral combination is achieved by shifting all spectra to zero redshift and by normalizing individual spectra to the same 6μm AGN continuum flux density. To compare quantitatively the star formation contributions of NLS1 and BLS1 in the same zone, we treated the composite spectra in the same way used to define R for individual sources. We then define a variable describing the relative importance of star formation in NLS1 compared to BLS1, F_{SB} by

$$F_{SB} = \frac{R_{NLS1}(PAH,6.2)}{R_{BLS1}(PAH,6.2)}, \tag{4.2}$$

where $R_{NLS1}(PAH,6.2)$ and $R_{BLS1}(PAH,6.2)$ are the ratios of 6.2 μm PAH fluxes to 6 μm AGN continuum for the NLS1 and BLS1 average spectra, respectively. $F_{SB} > 1$ stands for a more intense SF activity in NLS1s compared to BLS1s. In Table 1 we list the measured values of R and F_{SB} in all ten zones. We emphasize that in all the bins but two, an enhanced NLS1 star formation activity is found by at least a factor $\gtrsim$ 2. Only one zone is an exception hosting no BLS1, due to the absence

of nearby low luminosity BLS1.

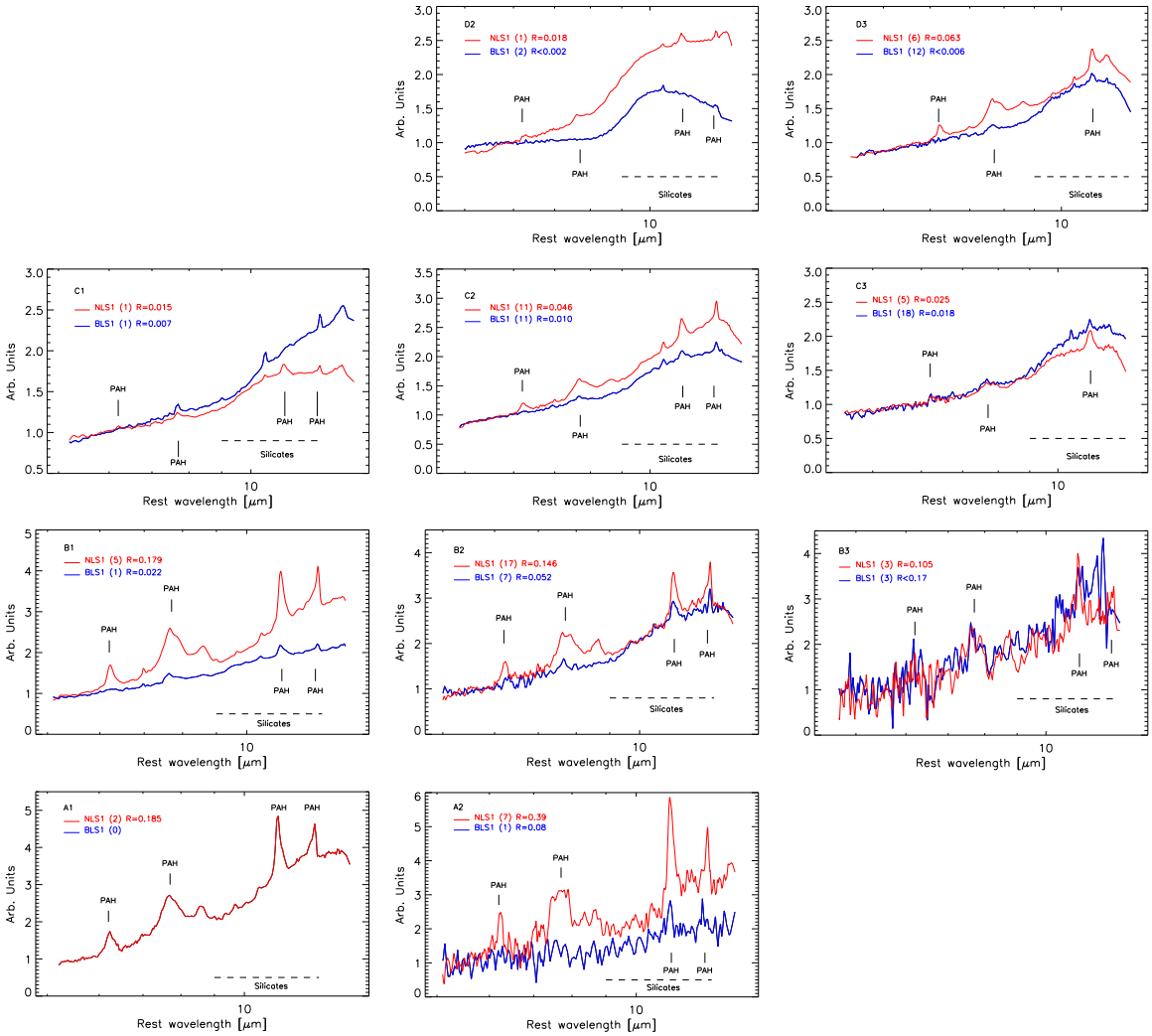

Figure 3: Average NLS1 spectra (red) compared with averaged BLS1 spectra (blue). The panels are arranged and labelled like the regions defined in the luminosity-distance diagram (Fig. 2). Each panels cites also the number of sources involved in the stacking procedure and the proper R values.

In conclusion, the NLS1 and BLS1 AGNs investigated here seem to represent two groups of type-I sources that differ in their star formation properties. This does not resemble an artifact of aperture or luminosity effects and seems to be an intrinsic property of the two sub-classes.

5. Discussion

We have demonstated an enhanced star formation activity in NLS1 galaxies compared to their broad line counterparts, and the enhancement factor (F_{SB}) does not appear to be affected by luminosity and distance effects. Here we compare the SF tracer with the AGN accretion parameters; that is, the 6.2 PAH luminosity -to- AGN continuum emission (R) is plotted as a function of the central

Zone	R (NLS1)	R (BLS1)	F_{SB}
A1	0.185±0.003	-	-
A2	0.387±0.012	0.085±0.012	4.6±0.8
B1	0.179±0.0024	0.022±0.001	8.2±0.4
B2	0.146 ± 0.004	0.052±0.003	2.8±0.2
B3	0.10±0.02	< 0.2	> 0.5
C1	0.015±0.001	0.007±0.001	2.2±0.2
C2	0.047±0.01	0.008±0.004	5.9±0.4
C3	0.025±0.001	0.014±0.002	1.8±0.3
D2	0.018±0.001	< 0.001	> 20
D3	0.063±0.001	0.003±0.001	24±9

Table 1: Star formation activity parameters for the ten stacking zones in Fig. 2: R (in units of 10^{-2}) and F_{SB} are shown with propagated errors. The errors on F_{SB} are statistical, the dispersion of the data is not taken into account.

black hole mass and Eddington ratio. Black hole masses and accretion rates are computed by the single-epoch mass determination method based on the Kaspi et al. [7] Broad Line Region size vs 5100 monochromatic luminosity (R_{BLR}-$\lambda L_\lambda(5100)$) relation. Thus, the BLR size is estimated from the measured $\lambda L_\lambda(5100)$, and the mass estimate follows from assuming Keplerian motion of the Hβ emitting gas. The reverberation mapping-based scaling relations adopted here are [8]:

$$M_{BH} = 1.05 \times 10^8 \left(\frac{L_{5100}}{10^{46} erg/s} \right)^{0.65} \left[\frac{FWHM(H\beta)}{1000\ km/s} \right]^2 M_\odot \tag{5.1}$$

and

$$L/L_{Edd} = \frac{f L_{5100}}{1.5 \times 10^{38} [M_{BH}/M_\odot]} \tag{5.2}$$

for BH mass and accretion rate respectively and where L_{5100} stands for the 5100 monochromatic luminosity. In this equation f is the bolometric correction factor. For low- to intermediate-luminosity AGN, this factor is between 7 and 12 [9] and is possibly luminosity dependent. Hence, bolometric luminosities were calculated from the monochromatic luminosities (L_{5100}), by using the correction factors of Marconi et al. (2004). These M_{BH} (and thus L/L_{Edd}) values are considered to be accurate to within a factor of $\sim 2-3$.

Figure 4 displays the bi-dimensional SF vs AGN properties plots. As seen in the left panel of this figure, the SF activity increases with decreasing BH masses, and moreover, the region of low BH masses and highest R values ($\mathrm{Log}(M_{BH}/M_\odot) < 7$ and $R \gtrsim 10^{-2}$) is populated by NLS1s with the complete absence of BLS1. Another interesting result is found also in the Fig. 4 right panel, where the R value increases with the Eddington ratio, i.e. the AGN luminosity expressed in terms of the Eddington luminosity. Also, in this case, NLS1 are the only AGNs populating the region of the extreme measurements of both SF activity and Eddington ratio.

The upper limits in R make us refrain from expressing this trend in terms of a quantitative scaling relation between star formation activity and Eddington ratio. Nevertheless, our plots demonstrate the supposed intimate correlation between the circumnuclear (within few central kpc) star

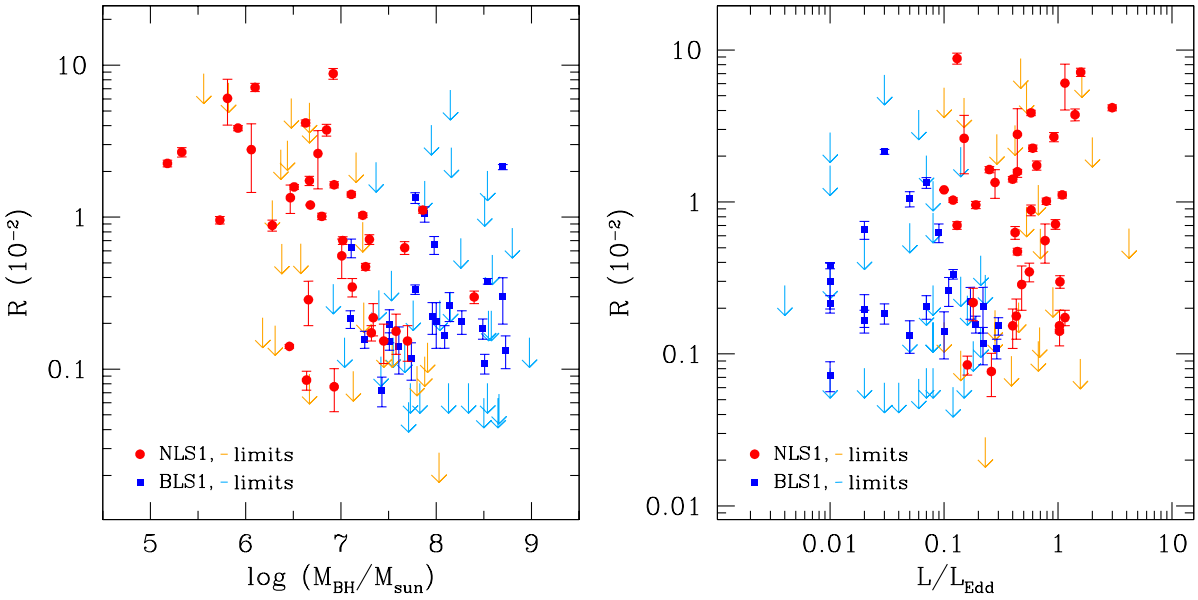

Figure 4: PAH-to-AGN continuum ratio R as a function of the central SMBH parameters. Symbols are as in Fig. 1. *Left panel*: R values versus central BH mass. *Right panel:* R values versus Eddington luminosity ratio. The BH masses and Eddington Rations are computed according to Netzer & Trakhtenbrot [8], see text for details.

formation and the AGN fuelling. The NLS1 galaxies are characterized by smaller BH mass, larger Eddington ratio and stronger SF activity compared to their broad line counterparts. Thus, we can safely conclude that AGN with the higher accretion efficiency are surrounded by more intense star formation than the less violently accreting super massive BH in the local Universe.

The results shown here are described in Sani et al. [10].

References

[1] B. M. Peterson, I. M. McHardy, B. J. Wilkes, *Variability of NGC 4051 and the nature of narrow-line Seyfert 1 galaxies Ne wAR*, **44**, 491, 2000

[2] D. Grupe, *A Complete Sample of Soft X-Ray-selected AGNs. II. Statistical Analysis*, *AJ*, **127**, 1799, 2004

[3] O. Shemmer, H. Netzer, R. Maiolino, E. Oliva, S. Croom, E. Corbett, L. di Fabrizio, *Near-Infrared Spectroscopy of High-Redshift Active Galactic Nuclei. I. A Metallicity-Accretion Rate Relationship*, *ApJ*, **614**, 547, 2004

[4] S. Mathur, *Narrow-line Seyfert 1 galaxies and the evolution of galaxies and active galaxies*, *ApJ*, **314**, 17, 2004

[5] M.-P. Véron-Cetty, P. Véron, *A catalogue of quasars and active nuclei: 12th edition*, *A&A*, **455**, 773, 2006

[6] M. Schweitzer, D. Lutz, E. Sturm, A. Contursi, L. J. Tacconi, M. D. Lehnert, K. M. Dasyra, R. Genzel, S. Veilleux, D. Rupke, *Spitzer Quasar and ULIRG Evolution Study (QUEST). I. The Origin of the Far-Infrared Continuum of QSOs*, *ApJ*, **649**, 79, 2006

[7] S. Kaspi, D. Maoz, H. Netzer, B. M. Peterson, M. Vestergaard, B. T. Jannuzi, *The Relationship between Luminosity and Broad-Line Region Size in Active Galactic Nuclei*, *ApJ*, **629**, 61, 2005

[8] H. Netzer, B. Trackhtenbrot, *Cosmic Evolution of Mass Accretion Rate and Metallicity in Active Galactic Nuclei*, *ApJ*, **654**, 754, 2007

[9] A. Marconi, G. Risaliti, R. Gilli, L. K. Hunt, R. Maiolino, M. Salvati, *Local supermassive black holes, relics of active galactic nuclei and the X-ray background*, *MNRAS*, **351**, 169, 2004

[10] E. Sani, D. Lutz, G. Risaliti, H. Netzer, L. Gallo, B. Trackhtenbrot, E. Sturm, T. Boller, *Enhanced star formation in narrow-line Seyfert 1 active galactic nuclei revealed by Spitzer*, *MNRAS*, **403**, 1246, 2010